Received: 19 August 2020

DOI: 10.1002/mma.7065

SPECIAL ISSUE PAPER

WILEY

A study on fractional COVID-19 disease model by using Hermite wavelets

Sunil Kumar[1,2] | **Ranbir Kumar**[1] | **Shaher Momani**[2,3] | **Samir Hadid**[2,4]

[1]Department of Mathematics, National Institute of Technology, Jamshedpur, Jharkhand, India

[2]Nonlinear Dynamics Research Center (NDRC), Ajman University, Ajman, UAE

[3]Department of Mathematics, Faculty of Science, University of Jordan, Amman, Jordan

[4]Department of Mathematics and Sciences, College of Humanities and Sciences, Ajman University, Ajman, UAE

Correspondence
Sunil Kumar, Department of Mathematics, National Institute of Technology, Jamshedpur 831014, Jharkhand, India.
Email: skumar.rs.apm@itbhu.ac.in

Communicated by: D. Baleanu

Funding information
Ajman University, Grant/Award Number: 2020-COVID-19-07

The preeminent target of present study is to reveal the speed characteristic of ongoing outbreak COVID-19 due to novel coronavirus. On January 2020, the novel coronavirus infection (COVID-19) detected in India, and the total statistic of cases continuously increased to 7 128 268 cases including 109 285 deceases to October 2020, where 860 601 cases are active in India. In this study, we use the Hermite wavelets basis in order to solve the COVID-19 model with time-arbitrary Caputo derivative. The discussed framework is based upon Hermite wavelets. The operational matrix incorporated with the collocation scheme is used in order to transform arbitrary-order problem into algebraic equations. The corrector scheme is also used for solving the COVID-19 model for distinct value of arbitrary order. Also, authors have investigated the various behaviors of the arbitrary-order COVID-19 system and procured developments are matched with exiting developments by various techniques. The various illustrations of susceptible, exposed, infected, and recovered individuals are given for its behaviors at the various value of fractional order. In addition, the proposed model has been also supported by some numerical simulations and wavelet-based results.

KEYWORDS

Caputo derivative, convergence analysis, coronavirus, Hermite wavelets, mathematical model, operational matrix

MSC CLASSIFICATION

26A33; 34A08; 34A34; 60G22

1 | INTRODUCTION

The coronavirus infection (COVID-19) is the most deadly and dangerous infectious infection in the whole globe. The COVID-19 infection, the short form of corona virus infection (2019), is sourced by serious intense respiratory syndrome corona virus 2 (SARS-CoV-2).[1] Most individual infected red to the COVID-19 infection will experience mild to mitigate respiratory sickness and instaurate without requiring special treatment. The outbreak of a harmful and extremely infected virus of the current period is a corona infection, and it is recognized first time in the Wuhan place (China) on December 2019.[2] In January 2020, the World Health Organization (WHO) divulged the COVID-19 infection to be a social fitness difficulty and recognized it as a outbreak on 11 March 2020. Since then, it killed over 1 61 402 on April 19 over the infected case of 23 47 875 individuals in more than 180 countries. From the starting up to the present day, there is no drug or dose available to completely recovered infected individual. In the initial stages of this infectious infection outbreak, patients feel tiredness, dry cough, and fever sometimes lead to breathing problems. Recently, Lin et al. discussed an accurate system for the COVID-19 infection, which accurately captures the time line of the COVID-19 infection in Lin et al.[3]

In 2020, Chen et al.[4] discussed a mathematical system for reproducing the stage-based transmission of the COVID-19 infection. Recently, Khan et al.[5] formulated mathematical system to study on the COVID-19 infection. In maximum cases, the infected individuals have few same symptoms which combine dry cough (68%) and fever (88%). Few of the cases have symptoms that combine tissue and joint pain, fatigue, respiratory sputum manufacture, sore throat, and headache. The COVID-19 infection disperses at a broad intensity between individual in the close touch with infected individual. According to WHO, the most common incubation period areas to 1–14 days.[6] In 2020, many researchers devoted themselves to study about COVID-19 in previous studies.[7-10,10] The recorded cases of SARS-Cov-2, to 1 April 2020, till 18 April 2020, in India has been shown in Figure 1, and comparison between the number of recovered individual and number of deaths is displayed in Figure 2. Fractional calculus (FC) is dealing with the calculus of derivatives and integral of arbitrary-order real or complex.[11-27]

There has been a powerful development in fractional differential equations (FDEs) in last decades due to its popularity in distinct research areas of science and technology. FDEs have an advantage in modelling real-life phenomena because it will reduce the errors arising from the ignored parameters. There are numerous examples of the mathematical model, which are consists of FDEs. To mention some, FDEs are used in breast cancer,[28] hepatitis B virus,[29] and Nipah Virus.[30] The dengue model is discussed through FDEs in Kilicman and Hamdan,[31] and in Dubey et al.,[32] Baba and Ghanbari,[33] and Gao et al.[34] the food chain model, tuberculosis, and rubella, respectively.

In the present article, we are discussing the dynamics of the COVID-19 infection system recommended by Khan et al.[5] with time fractional Caputo derivative.

$$\begin{cases} {}_0^C D_t^\alpha \mathcal{S}(t) = \Delta - \lambda \mathcal{S} - \frac{\varphi \mathcal{S}(\mathcal{I}+\beta\mathcal{A})}{\mathcal{N}} - \gamma \mathcal{S}\mathcal{Q}, \\ {}_0^C D_t^\alpha \mathcal{E}(t) = \frac{\varphi \mathcal{S}(\mathcal{I}+\beta\mathcal{A})}{\mathcal{N}} + \gamma \mathcal{S}\mathcal{Q} - (1-\theta)\delta\mathcal{E} - \theta\mu\mathcal{E} - \lambda\mathcal{E}, \\ {}_0^C D_t^\alpha \mathcal{I}(t) = (1-\theta)\delta\mathcal{E} - (\sigma+\lambda)\mathcal{I}, \\ {}_0^C D_t^\alpha \mathcal{A}(t) = \theta\mu\mathcal{E} - (\rho+\lambda)\mathcal{A}, \\ {}_0^C D_t^\alpha \mathcal{R}(t) = \sigma\mathcal{I} + \rho\mathcal{A} - \lambda\mathcal{R}, \\ {}_0^C D_t^\alpha \mathcal{Q}(t) = \xi\mathcal{I} + \zeta\mathcal{A} - \eta\mathcal{Q}, \end{cases} \tag{1}$$

with primary conditions $\mathcal{S}(0) = \omega_1$, $\mathcal{E}(0) = \omega_2$, $\mathcal{I}(0) = \omega_3$, $\mathcal{A}(0) = \omega_4$, $\mathcal{R}(0) = \omega_5$ and $\mathcal{Q}(0) = \omega_6$, where $\mathcal{N}$ is the overall population of individual. Again, $\mathcal{N}$ divided into five subpart in the manner that susceptible individual $\mathcal{S}(t)$, exposed individual $\mathcal{E}(t)$, infected (symptomatic) individual $\mathcal{I}(t)$, asymptotically infected $\mathcal{A}(t)$, and the recovered or the removed individual $\mathcal{R}(t)$. The individual of the market or reservoir is stand for $\mathcal{Q}(t)$.

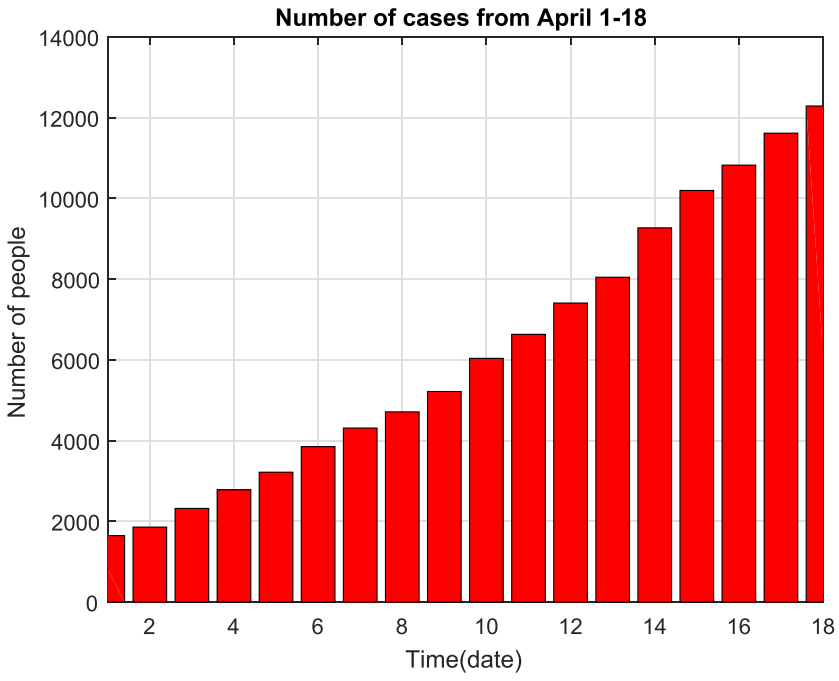

FIGURE 1 Plot of recovered people and number of deaths during 1 April–18 April 2020 in India [Colour figure can be viewed at wileyonlinelibrary.com]

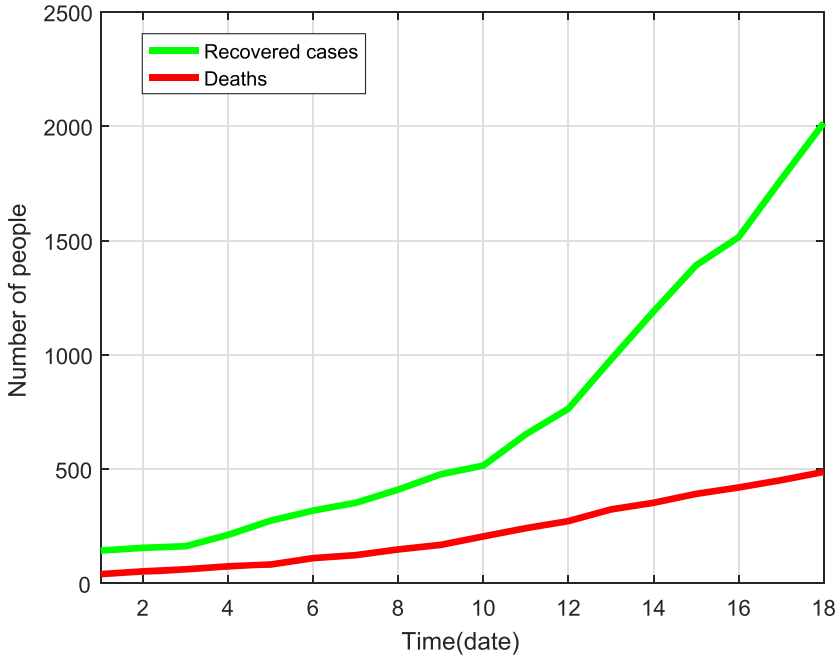

FIGURE 2 Plot of recovered people and number of deaths during 1 April–18 April 2020 in India [Colour figure can be viewed at wileyonlinelibrary.com]

During the 1980s, wavelet analysis because of their outstanding application in image and signal processing became popular tools in many branches of science and engineering. More than that, speciality such as orthogonality, good localization of wavelets have attracted many researchers. Wavelets sanction the precise representation of variety of operator and functions.[35,36] Therefore, wavelets have significant role in many fields like image processing, time frequency analysis, and signal processing.[37] Basis of wavelet is relatively incipient and has received attention for solving various types of FDEs. Legendre, Hermite, and Laguerre wavelets are used to solve FDEs in previous studies.[38-41] The Bernoulli wavelet is used to solve coupled models of nonlinear arbitrary-order integro-DEs in Wang et al.[42] Recently, Kumar et al. have discussed Bernstein wavelets method for solving SIR epidemic.[43] There are some research articles on Hermite wavelets for solving FDEs.[44,45] Best of our knowledge, there is not any article based on Hermite wavelets for solving Biological models in $[0, t_l]$. The work is set up as pursue; in part 2, we provide some basic essential explanations of FC. In Part 3, we construct the Hermite wavelets for arbitrary interval and also discussed the convergence analysis. We develop the operational for Hermite wavelets with the help of block pulse functions in Part 4. In Part 5, we use Hermite wavelets and Adams–Bashforth–Moulton (ABM) to solve the COVID-19 infection model. Numerical simulation and discussion are given in Part 6. Finally, achieving remarks are given in Part 7.

2 | PRELIMINARIES

There are some essential explanations of arbitrary derivative and integral in previous studies.[46-48]

Definition 2.1. The Riemann–Liouville (RL) integral operator of order α is described as

$$I_t^{\alpha}\Upsilon(t) = \begin{cases} \frac{1}{\Gamma(\alpha)}\int_0^t \frac{\Upsilon(\tau)}{(t-\tau)^{1-\alpha}}d\tau = \frac{1}{\Gamma(\alpha)}t^{\alpha-1} * \Upsilon(t), \ \alpha > 0, t > 0, \\ \Upsilon(t), \ \alpha = 0, \end{cases} \tag{2}$$

where $t^{\alpha-1} * \Upsilon(t)$ is the convolution product of $t^{\alpha-1}$ and $\Upsilon(t)$.

Definition 2.2. Arbitrary-order derivative α in the sense of Caputo's is described as

$${}_0^C D_t^{\alpha}\Upsilon(t) = \left\{ \frac{1}{\Gamma(n-\alpha)}\int_0^t \frac{\Upsilon^{(n)}(\tau)}{(t-\tau)^{\alpha+1-n}}d\tau, \ n-1 < \alpha \le n, \ n \in N. \right. \tag{3}$$

3 | HERMITE WAVELETS FUNCTION AND ITS PROPERTIES

Let k, M be positive integer. The Hermite wavelets $\psi_{nm}(t)$ for $n = 1, 2, 3, \ldots, 2^{k-1}$ and $m = 0, 1, 2, \ldots, M-1$ are described on the interval $[0, t_l)$ as

$$\psi_{nm}(t) = \begin{cases} \frac{2^{\frac{k+1}{2}}}{\sqrt{\pi}} \mathcal{H}_m\left(\frac{2^k}{t_l} t - 2n + 1\right), \ if, \frac{2n-2}{2^k} t_l \le t < \frac{2n}{2^k} t_l, \\ 0, \ otherwise, \end{cases} \tag{4}$$

where $\mathcal{H}_m(t)$ is the well-known Hermite polynomial of degree m with respect to the weight function $w(t) = \sqrt{1-t^2}$ on the real line $\mathbb{R}$ and fulfill the following recurrence relation.

$$\mathcal{H}_0(t) = 1,$$

$$\mathcal{H}_1(t) = 2t,$$

$$\mathcal{H}_{m+2}(t) = 2t\mathcal{H}_{m+1}(t) - 2(m+1)\mathcal{H}_m(t).$$

Let $\Omega_{k,M}$ be the space spanned by Hermite wavelets for ψ_{nm}, that is, $\Omega_{k,M} = \text{span}\{\psi_{1,0}, \psi_{2,0}, \ldots, \psi_{2^{k-1},0}, \psi_{1,1}, \ldots, \psi_{2^{k-1},1}, \psi_{2,2}, \ldots, \psi_{2^{k-1},2}, \ldots, \psi_{2^{k-1},M}\} \subseteq L^2(0,1)$. Let Υ be an arbitrary element in $L^2(0,1)$. Then, Υ has particular perfect approximation out of $\Omega_{k,M}$ in the manner that $\Upsilon_0 \in \Omega_{k,M}$,

$$\forall \zeta \in \Omega_{k,M}, \qquad \|\Upsilon - \Upsilon_0\| \le \|\Upsilon - \zeta\|.$$

Since $\Upsilon_0 \in \Omega_{k,M}$ is the particular perfect approximation, then there exists particular coefficients $\Lambda_{1,0}, \Lambda_{2,0}, \ldots, \Lambda_{2^{k-1},0}, \Lambda_{1,1}, \ldots, \Lambda_{2^{k-1},1}, \Lambda_{2,2}, \ldots, \Lambda_{2^{k-1},2}, \ldots, \Lambda_{2^{k-1},M}$ in the manner that

$$\Upsilon(t) \simeq \Upsilon_0(t) = \sum_{n=1}^{2^{k-1}M-1} \sum_{m=0} \Lambda_{nm} \psi_{nm}(t) = \Lambda^T G, \tag{5}$$

where Λ and G vectors are defined as

$$\Lambda^T = [\Lambda_{1,0}, \Lambda_{2,0}, \ldots, \Lambda_{2^{k-1},0}, \Lambda_{1,1}, \ldots, \Lambda_{2^{k-1},1}, \Lambda_{2,2}, \ldots, \Lambda_{2^{k-1},2}, \ldots, \Lambda_{2^{k-1},M}]$$

and

$$G^T = [\psi_{1,0}, \psi_{2,0}, \ldots, \psi_{2^{k-1},0}, \psi_{1,1}, \ldots, \psi_{2^{k-1},1}, \psi_{2,2}, \ldots, \psi_{2^{k-1},2}, \ldots, \psi_{2^{k-1},M}].$$

Choosing $k = 2$, $M = 4$, and the collocation points as $t_i = 2i - 1/2\hat{m}$, $i = 1, 2, \ldots, \hat{m} = 2^{k-1}M$, we obtained the Hermite wavelets matrix as

$$\Phi_{8\times 8} = \begin{pmatrix} 1.5958 & 1.5958 & 1.5958 & 1.5958 & 0 & 0 & 0 & 0 \\ 0 & 0 & 0 & 0 & 1.5958 & 1.5958 & 1.5958 & 1.5958 \\ -2.3937 & -0.7979 & 0.7979 & 2.3937 & 0 & 0 & 0 & 0 \\ 0 & 0 & 0 & 0 & -2.3937 & -0.7979 & 0.7979 & 2.3937 \\ 0.3989 & -2.7926 & -2.7926 & 0.3989 & 0 & 0 & 0 & 0 \\ 0 & 0 & 0 & 0 & 0.3989 & -2.7926 & -2.7926 & 0.3989 \\ 9.6245 & 2.1443 & -4.9369 & -9.2255 & 0 & 0 & 0 & 0 \\ 0 & 0 & 0 & 0 & 10.0234 & -0.6483 & -7.7295 & -8.8266 \end{pmatrix}.$$

3.1 | Convergence analysis of Hermite wavelets approximation

Theorem 3.1. *Let $\Upsilon(t) \in L^2[0, t_l]$ be the function and $\Upsilon_0(t) \in \Omega_{k,M}$ is the approximation of $\Upsilon(t)$ then*

$$\|\epsilon_\Upsilon\| = \|\Upsilon(t) - \Upsilon_0(t)\| < \frac{\mathcal{B} t_l^{\frac{2M+1}{2}}}{M!\sqrt{2M+1}}.$$

Proof. Let $\Upsilon^{(i)}(t)$ be the continuous function, where $i = 0, 1, 2, \ldots M$. Then there exist $\mathcal{B} \in \mathbb{N}$ such that

$$\Upsilon^{(i)}(t) < \mathcal{B}, \ \forall \ t \in [0, t_l].$$

Then by Taylor′s formula

$$\Upsilon(t) = \sum_{i=0}^{M-1} \frac{\Upsilon^i(0)t^i}{i!} + \frac{\Upsilon^{(M)}(\xi)}{M!}t^M, \ \textit{where } \xi \in [0, t_l].$$

Since, $\{\psi_{nm}(t)\}$ is the family of piecewise function. As $\Omega_{k,M} = span\{\psi_{nm}(t)\}$, therefore

$$\sum_{0}^{M-1} \frac{\Upsilon^{(i)}(0)t^i}{i!} \in \Omega_{k,M},$$

as $\Upsilon_0(t)$ is the favorite approximation of $\Upsilon(t)$ out of $\Omega_{k,M}$, then

$$\begin{aligned}
\|\epsilon_\Upsilon\| &= \|\Upsilon(t) - \Upsilon_0(t)\| \\
&\leq \left\| \Upsilon(t) - \sum_{0}^{M-1} \frac{\Upsilon^{(i)}(0)t^i}{i!} \right\| \\
&= \left\| \frac{\Upsilon^{(M)}(\xi)t^M}{M!} \right\| \\
&= \left(\int_0^{t_l} \left(\frac{\Upsilon^{(M)}(\xi)t^M}{M!} \right)^2 \right)^{\frac{1}{2}} \\
&< \left(\frac{\mathcal{B}^2 t_l^{2M+1}}{(M!)^2(2M+1)} \right)^{\frac{1}{2}} \\
&= \frac{\mathcal{B}t_l^{\frac{2M+1}{2}}}{M!\sqrt{2M+1}}
\end{aligned}$$

where $t_l \in \mathbb{N}$ is the fixed number and when M is sufficiently large then $\|\epsilon_\Upsilon\| \to 0$. Hence, Hermite wavelets approximation is convergent. □

4 | HERMITE WAVELETS OPERATIONAL MATRIX

In the following section, the Hermite wavelets operational matrix for integer-order integration and fractional-order integration, respectively, are obtained. These operational matrices play vital role in the proposed method for solving the problem.

4.1 | The BPFs

The block pulse functions (BPFs) defined over the interval $[0, t_l)$ as

$$b_j(t) = \begin{cases} 1, \ if, \ \frac{jt_l}{\hat{m}} \leq t < \frac{(j+1)t_l}{\hat{m}}, \\ 0, \ otherwise, \end{cases} \tag{6}$$

where $j = 0, 1, 2, \dots, \widehat{m}$ and $\mathcal{B}_{\widehat{m}} = [b_1, b_2, b_3, \dots, b_{\widehat{m}}]$. The useful properties of BPFs are listed in previous studies.[48-51] Here, we will use BPFs to construct the Hermite wavelets operational matrix of arbitrary-order integration.

$$(I_t^{\alpha}\mathcal{B}_{\widehat{m}})(t) \cong F^{\alpha}\mathcal{B}_{\widehat{m}},$$

$$F^{\alpha}_{\widehat{m}\times\widehat{m}} = \frac{t_l^{\alpha}}{\widehat{m}^{\alpha}\Gamma(\alpha+2)}\begin{pmatrix} 1 & \zeta_1 & \zeta_2 & \zeta_3 & \dots & \zeta_{\widehat{m}-1} \\ 0 & 1 & \zeta_1 & \zeta_2 & \dots & \zeta_{\widehat{m}-2} \\ 0 & 0 & 1 & \zeta_1 & \dots & \zeta_{\widehat{m}-3} \\ \vdots & \vdots & \ddots & \ddots & & \vdots \\ 0 & 0 & \dots & 0 & 1 & \zeta_1 \\ 0 & 0 & \dots & 0 & 0 & 1 \end{pmatrix}. \tag{7}$$

and $\zeta_l = (l+1)^{\alpha+1} - 2l^{\alpha+1} + (l-1)^{\alpha+1}$, for $l = 1, 2, 3, \dots, m \hat{-} 1$.

Now, we develop the Genocchi wavelets operational matrix for arbitrary-order integration, P^{α}. Let

$$(I_t^{\alpha}\Psi)(t) \cong P^{\alpha}\Psi(t).$$

Then,

$$(I_t^{\alpha}\Psi)(t) \cong (I_t^{\alpha}\Psi\mathcal{B}_{\widehat{m}})(t) = \Psi(I_t^{\alpha}\mathcal{B}_{\widehat{m}})(t) \approx \Psi F^{\alpha}\mathcal{B}_{\widehat{m}}.$$

Hence,

$$p^{\alpha}\Psi(t) \cong \Psi(t)F^{\alpha}\mathcal{B}_{\widehat{m}}$$

$$p^{\alpha} = \phi_{m\hat{\times}\widehat{m}}F^{\alpha}\phi^{-1}_{m\hat{\times}\widehat{m}}.$$

Using the above fact the operational matrix, P^{α} for $\alpha = 0.5$, $M = 4$, $k = 2$, and $t_l = 1$ is given as

$$P^{\alpha}_{8\times 8} = \begin{pmatrix} 0.5124 & 0.4576 & 0.2897 & -0.2029 & -0.0426 & 0.0703 & 0.0330 & -0.0318 \\ 0 & 0.5124 & 0 & 0.2897 & 0 & -0.0755 & 0 & 0.0330 \\ -0.1003 & 0.1119 & -0.1758 & -0.2013 & 0.1804 & 0.0795 & -0.1007 & -0.0382 \\ 0 & -0.1003 & 0 & -0.1758 & 0 & 0.2811 & 0 & -0.1007 \\ -0.2842 & -0.3129 & 1.3904 & 0.0541 & -0.0145 & -0.0123 & 0.4045 & 0.0037 \\ 0 & -0.2842 & 0 & 1.3904 & 0 & -0.4191 & 0 & 0.4045 \\ 0.2478 & -0.6013 & 1.9440 & 0.8241 & -0.8078 & -0.3208 & 0.7418 & 0.1528 \\ 0 & -0.0364 & 0 & 3.3344 & 0 & -1.9687 & 0 & 1.1464 \end{pmatrix}.$$

This is the operational matrix of BPFs of 8×8 order.

5 | PROPOSED METHODS

We have formulated proposed schemes for the study of arbitrary-order COVID-19 infection system.

5.1 | The Hermite wavelets for arbitrary-order COVID-19 infection system

Let us consider a fractional model of arbitrary-order COVID-19 infection system as

$$\begin{cases} {}_0^C D_t^{\alpha}\mathcal{S}(t) = {}^1\Lambda_{\widehat{m}}^T\Psi_{\widehat{m}}(t), \\ {}_0^C D_t^{\alpha}\mathcal{E}(t) = {}^2\Lambda_{\widehat{m}}^T\Psi_{\widehat{m}}(t), \\ {}_0^C D_t^{\alpha}\mathcal{I}(t) = {}^3\Lambda_{\widehat{m}}^T\Psi_{\widehat{m}}(t), \\ {}_0^C D_t^{\alpha}\mathcal{A}(t) = {}^4\Lambda_{\widehat{m}}^T\Psi_{\widehat{m}}(t), \\ {}_0^C D_t^{\alpha}\mathcal{R}(t) = {}^5\Lambda_{\widehat{m}}^T\Psi_{\widehat{m}}(t), \\ {}_0^C D_t^{\alpha}\mathcal{Q}(t) = {}^6\Lambda_{\widehat{m}}^T\Psi_{\widehat{m}}(t), \end{cases} \tag{8}$$

where ${}^{l}\Lambda_{\hat{m}}^{T} = [{}^{l}\Lambda_1, {}^{l}\Lambda_2, {}^{l}\Lambda_3 \ \dots \ , {}^{l}\Lambda_{\hat{m}}]$, $l = 1, 2, 3, 4, 5, 6$ are unknown coefficients. By using the primary conditions and definition of arbitrary-order integral operator, we obtain

$$\begin{cases} \mathcal{S}(t) = I_t^{\alpha}\, {}_0^C D_t^{\alpha} \mathcal{S}(t) + \mathcal{S}(0) \approx {}^{1}\Lambda_{\hat{m}}^{T} P_{\hat{m}\times\hat{m}}^{\alpha} \Psi_{\hat{m}}(t) + \mathcal{S}(0), \\ \mathcal{E}(t) = I_t^{\alpha}\, {}_0^C D_t^{\alpha} \mathcal{E}(t) + \mathcal{E}(0) \approx {}^{2}\Lambda_{\hat{m}}^{T} P_{\hat{m}\times\hat{m}}^{\alpha} \Psi_{\hat{m}}(t) + \mathcal{E}(0), \\ \mathcal{I}(t) = I_t^{\alpha}\, {}_0^C D_t^{\alpha} \mathcal{I}(t) + \mathcal{I}(0) \approx {}^{3}\Lambda_{\hat{m}}^{T} P_{\hat{m}\times\hat{m}}^{\alpha} \Psi_{\hat{m}}(t) + \mathcal{I}(0), \\ \mathcal{A}(t) = I_t^{\alpha}\, {}_0^C D_t^{\alpha} \mathcal{A}(t) + \mathcal{A}(0) \approx {}^{4}\Lambda_{\hat{m}}^{T} P_{\hat{m}\times\hat{m}}^{\alpha} \Psi_{\hat{m}}(t) + \mathcal{A}(0), \\ \mathcal{R}(t) = I_t^{\alpha}\, {}_0^C D_t^{\alpha} \mathcal{R}(t) + \mathcal{R}(0) \approx {}^{5}\Lambda_{\hat{m}}^{T} P_{\hat{m}\times\hat{m}}^{\alpha} \Psi_{\hat{m}}(t) + \mathcal{R}(0), \\ \mathcal{Q}(t) = I_t^{\alpha}\, {}_0^C D_t^{\alpha} \mathcal{Q}(t) + \mathcal{Q}(0) \approx {}^{6}\Lambda_{\hat{m}}^{T} P_{\hat{m}\times\hat{m}}^{\alpha} \Psi_{\hat{m}}(t) + \mathcal{Q}(0). \end{cases} \tag{9}$$

Further, using the properties of BPFs in (9), we obtain

$$\begin{cases} \mathcal{S}(t) = {}^{1}\Lambda_{\hat{m}}^{T} P_{\hat{m}\times\hat{m}}^{\alpha} \Phi_{\hat{m}\times\hat{m}} \mathcal{B}_{\hat{m}} + \mathcal{S}(0), \\ \mathcal{E}(t) = {}^{2}\Lambda_{\hat{m}}^{T} P_{\hat{m}\times\hat{m}}^{\alpha} \Phi_{\hat{m}\times\hat{m}} \mathcal{B}_{\hat{m}} + \mathcal{E}(0), \\ \mathcal{I}(t) = {}^{3}\Lambda_{\hat{m}}^{T} P_{\hat{m}\times\hat{m}}^{\alpha} \Phi_{\hat{m}\times\hat{m}} \mathcal{B}_{\hat{m}} + \mathcal{I}(0), \\ \mathcal{A}(t) = {}^{4}\Lambda_{\hat{m}}^{T} P_{\hat{m}\times\hat{m}}^{\alpha} \Phi_{\hat{m}\times\hat{m}} \mathcal{B}_{\hat{m}} + \mathcal{A}(0), \\ \mathcal{R}(t) = {}^{5}\Lambda_{\hat{m}}^{T} P_{\hat{m}\times\hat{m}}^{\alpha} \Phi_{\hat{m}\times\hat{m}} \mathcal{B}_{\hat{m}} + \mathcal{R}(0), \\ \mathcal{Q}(t) = {}^{6}\Lambda_{\hat{m}}^{T} P_{\hat{m}\times\hat{m}}^{\alpha} \Phi_{\hat{m}\times\hat{m}} \mathcal{B}_{\hat{m}} + \mathcal{Q}(0). \end{cases} \tag{10}$$

Then, we have

$$\begin{aligned} \mathcal{S}(t)\mathcal{I}(t) &= ({}^{1}\Lambda_{\hat{m}}^{T} P_{\hat{m}\times\hat{m}}^{\alpha} \Phi_{\hat{m}\times\hat{m}} \mathcal{B}_{\hat{m}} + \mathcal{S}(0))({}^{3}\Lambda_{\hat{m}}^{T} P_{\hat{m}\times\hat{m}}^{\alpha} \Phi_{\hat{m}\times\hat{m}} \mathcal{B}_{\hat{m}} + \mathcal{I}(0)) \\ &= ({}^{1}\Lambda_{\hat{m}}^{T} P_{\hat{m}\times\hat{m}}^{\alpha} \Phi_{\hat{m}\times\hat{m}} \otimes {}^{3}\Lambda_{\hat{m}}^{T} P_{\hat{m}\times\hat{m}}^{\alpha} \Phi_{\hat{m}\times\hat{m}}) \mathcal{B}_{\hat{m}} \\ &\quad + \mathcal{I}(0) {}^{1}\Lambda_{\hat{m}}^{T} P_{\hat{m}\times\hat{m}}^{\alpha} \Phi_{\hat{m}\times\hat{m}} + \mathcal{S}(0) {}^{3}\Lambda_{\hat{m}}^{T} P_{\hat{m}\times\hat{m}}^{\alpha} \Phi_{\hat{m}\times\hat{m}} \mathcal{B}_{\hat{m}} \\ &\quad + \mathcal{S}(0)\mathcal{I}(0)[1, 1, \ \dots \ , 1]_{1\times\hat{m}} \mathcal{B}_{\hat{m}}, \end{aligned} \tag{11}$$

and

$$\begin{aligned} \mathcal{S}(t)\mathcal{Q}(t) &= ({}^{1}\Lambda_{\hat{m}}^{T} P_{\hat{m}\times\hat{m}}^{\alpha} \Phi_{\hat{m}\times\hat{m}} \mathcal{B}_{\hat{m}} + \mathcal{S}(0))({}^{6}\Lambda_{\hat{m}}^{T} P_{\hat{m}\times\hat{m}}^{\alpha} \Phi_{\hat{m}\times\hat{m}} \mathcal{B}_{\hat{m}} + \mathcal{Q}(0)) \\ &= ({}^{1}\Lambda_{\hat{m}}^{T} P_{\hat{m}\times\hat{m}}^{\alpha} \Phi_{\hat{m}\times\hat{m}} \otimes {}^{6}\Lambda_{\hat{m}}^{T} P_{\hat{m}\times\hat{m}}^{\alpha} \Phi_{\hat{m}\times\hat{m}}) \mathcal{B}_{\hat{m}} \\ &\quad + \mathcal{Q}(0) {}^{1}\Lambda_{\hat{m}}^{T} P_{\hat{m}\times\hat{m}}^{\alpha} \Phi_{\hat{m}\times\hat{m}} + \mathcal{S}(0) {}^{6}\Lambda_{\hat{m}}^{T} P_{\hat{m}\times\hat{m}}^{\alpha} \Phi_{\hat{m}\times\hat{m}} \mathcal{B}_{\hat{m}} \\ &\quad + \mathcal{S}(0)\mathcal{Q}(0)[1, 1, \ \dots \ , 1]_{1\times\hat{m}} \mathcal{B}_{\hat{m}}. \end{aligned} \tag{12}$$

Now, we substitute Equations (8), (10), (11), and (12) into the COVID-19 model (1) of fractional order; we obtain the system of algebraic equations. By adopting, Newton iteration method to solve nonlinear algebraic equations; we can find the anonymous coefficients. On substituting anonymous coefficients into the (10), we can achieve the required solutions.

5.2 | The ABM predictor corrector scheme for COVID-19 model

Here, mainly we will describe that famous numerical scheme ABM method as a pair to construct a predictor–corrector method to solve arbitrary-order COVID-19 infection system. On applying ABM method[52,53] on Equation (1), we obtained the predictor values and the corresponding corrector values as follows. To change it into discrete form, let $h = t_l - 0/\hat{m}$, $t_n = nh$, $n = 0, 1, 2, \ \dots \ , \hat{m} - 1$, and $\alpha \in (0, 1]$

$$\begin{aligned}
\mathcal{S}_{n+1} =& \mathcal{S}(0) + \frac{h^\alpha}{\Gamma(\alpha+2)}\left(\Delta - \lambda \mathcal{S}^p_{n+1} - \frac{\varphi \mathcal{S}^p_{n+1}(\mathcal{I}^p_{n+1} + \beta \mathcal{A}^p_{n+1})}{\mathcal{N}} - \gamma \mathcal{S}^p_{n+1}\mathcal{Q}^p_{n+1}\right) \\
&+ \frac{h^\alpha}{\Gamma(\alpha+2)}\sum_{j=0}^{n} a_{j,n+1}\left(\Delta - \lambda \mathcal{S}_j - \frac{\varphi \mathcal{S}_j(\mathcal{I}_j + \beta \mathcal{A}_j)}{\mathcal{N}} - \gamma \mathcal{S}_j\mathcal{Q}_j\right), \\
\mathcal{E}_{n+1} =& \mathcal{E}(0) + \frac{h^\alpha}{\Gamma(\alpha+2)}\left(\frac{\varphi \mathcal{S}^p_{n+1}(\mathcal{I}^p_{n+1} + \beta \mathcal{A}^p_{n+1})}{\mathcal{N}} + \gamma \mathcal{S}^p_{n+1}\mathcal{Q}^p_{n+1} - (1-\theta)\delta \mathcal{E}^p_{n+1} - \theta\mu \mathcal{E}^p_{n+1} - \lambda \mathcal{E}^p_{n+1}\right) \\
&+ \frac{h^\alpha}{\Gamma(\alpha+2)}\sum_{j=0}^{n} a_{j,n+1}\left(\frac{\varphi \mathcal{S}_j(\mathcal{I}_j + \beta \mathcal{A}_j)}{\mathcal{N}} + \gamma \mathcal{S}_j\mathcal{Q}_j - (1-\theta)\delta \mathcal{E}_j - \theta\mu \mathcal{E}_j - \lambda \mathcal{E}_j\right), \\
\mathcal{I}_{n+1} =& \mathcal{I}(0) + \frac{h^\alpha}{\Gamma(\alpha+2)}\left((1-\theta)\delta \mathcal{E}^p_{n+1} - (\sigma+\lambda)\mathcal{I}^p_{n+1}\right) \\
&+ \frac{h^\alpha}{\Gamma(\alpha+2)}\sum_{j=0}^{n} a_{j,n+1}\left((1-\theta)\delta \mathcal{E}_j - (\sigma+\lambda)\mathcal{I}_j\right), \\
\mathcal{A}_{n+1} =& \mathcal{A}(0) + \frac{h^\alpha}{\Gamma(\alpha+2)}\left(\theta\mu \mathcal{E}^p_{n+1} - (\rho+\lambda)\mathcal{A}^p_{n+1}\right) + \frac{h^\alpha}{\Gamma(\alpha+2)}\sum_{j=0}^{n} a_{j,n+1}\left(\theta\mu \mathcal{E}_j - (\rho+\lambda)\mathcal{A}_j\right), \\
\mathcal{R}_{n+1} =& \mathcal{R}(0) + \frac{h^\alpha}{\Gamma(\alpha+2)}\left(\sigma \mathcal{I}^p_{n+1} + \rho \mathcal{A}^p_{n+1} - \lambda \mathcal{R}^p_{n+1}\right) + \frac{h^\alpha}{\Gamma(\alpha+2)}\sum_{j=0}^{n} a_{j,n+1}\left(\sigma \mathcal{I}_j + \rho \mathcal{A}_j - \lambda \mathcal{R}_j\right), \\
\mathcal{Q}_{n+1} =& \mathcal{Q}(0) + \frac{h^\alpha}{\Gamma(\alpha+2)}\left(\xi \mathcal{I}^p_{n+1} + \zeta \mathcal{A}^p_{n+1} - \eta \mathcal{Q}^p_{n+1}\right) + \frac{h^\alpha}{\Gamma(\alpha+2)}\sum_{j=0}^{n} a_{j,n+1}\left(\xi \mathcal{I}_j + \zeta \mathcal{A}_j - \eta \mathcal{Q}_j\right), \\
\mathcal{S}^p_{n+1} =& \mathcal{S}(0) + \frac{1}{\Gamma(\alpha)}\sum_{j=0}^{n} b_{j,n+1}\left(\Delta - \lambda \mathcal{S}_j - \frac{\varphi \mathcal{S}_j(\mathcal{I}_j + \beta \mathcal{A}_j)}{\mathcal{N}} - \gamma \mathcal{S}_j\mathcal{Q}_j\right), \\
\mathcal{E}^p_{n+1} =& \mathcal{E}(0) + \frac{1}{\Gamma(\alpha)}\sum_{j=0}^{n} b_{j,n+1}\left(\frac{\varphi \mathcal{S}_j(\mathcal{I}_j + \beta \mathcal{A}_j)}{\mathcal{N}} + \gamma \mathcal{S}_j\mathcal{Q}_j - (1-\theta)\delta \mathcal{E}_j - \theta\mu \mathcal{E}_j - \lambda \mathcal{E}_j\right), \\
\mathcal{I}^p_{n+1} =& \mathcal{I}(0) + \frac{1}{\Gamma(\alpha)}\sum_{j=0}^{n} b_{j,n+1}\left((1-\theta)\delta \mathcal{E}_j - (\sigma+\lambda)\mathcal{I}_j\right), \\
\mathcal{A}^p_{n+1} =& \mathcal{A}(0) + \frac{1}{\Gamma(\alpha)}\sum_{j=0}^{n} b_{j,n+1}\left(\theta\mu \mathcal{E}_j - (\rho+\lambda)\mathcal{A}_j\right), \\
\mathcal{R}^p_{n+1} =& \mathcal{R}(0) + \frac{1}{\Gamma(\alpha)}\sum_{j=0}^{n} b_{j,n+1}\left(\sigma \mathcal{I}_j + \rho \mathcal{A}_j - \lambda \mathcal{R}_j\right), \\
\mathcal{Q}^p_{n+1} =& \mathcal{Q}(0) + \frac{1}{\Gamma(\alpha)}\sum_{j=0}^{n} b_{j,n+1}\left(\xi \mathcal{I}_j + \zeta \mathcal{A}_j - \eta \mathcal{Q}_j\right),
\end{aligned}$$

where

$$a_{j,n+1} = \begin{cases} n^{\alpha+1} - (n-\alpha)(n+1)^\alpha, & if\ j = 0, \\ (n-j+2)^{\alpha+1} + (n-j)^{\alpha+1} - 2(n-j+1)^{\alpha+1}, & if\ 0 \le j \le n, \\ 1, & if\ j = 1, \end{cases}$$

$$b_{j,n+1} = \frac{h^\alpha}{\alpha}((n+1-j)^\alpha - (n-j)^\alpha), \ 0 \le j \le n.$$

This is the formulation of arbitrary-order COVID-19 infection system by using ABM scheme.

6 | NUMERICAL DEVELOPMENTS AND ARGUMENTS

The primary objective of proposed section is to present numerical simulation and graphical illustration of susceptible, exposed, infected, and recovered individuals of the arbitrary-order COVID-19 infection system. Further, we observed the many behaviors susceptible, exposed, infected, and recovered peoples in arbitrary-order COVID-19 infection system by using Hermite wavelet and ABM methods. A comparative study of the susceptible, exposed, infected, and recovered individuals is represented through portrayed 03-20.

Here, we consider the arbitrary-order COVID-19 infection system with primary cases $\mathcal{S}(0) = \omega_1 = 480021700$, $\mathcal{E}(0) = \omega_2 = 1724266$, $\mathcal{I}(0) = \omega_3 = 745$, $\mathcal{A}(0) = \omega_4 = 413$, $\mathcal{R}(0) = \omega_5 = 66$, and $\mathcal{Q}(0) = \omega_6 = 1000000$ and total primary public $\mathcal{N} = 481747192$, which is the 35% of the total public in India. Further, in 2019, the life expectancy in the India is 69.50

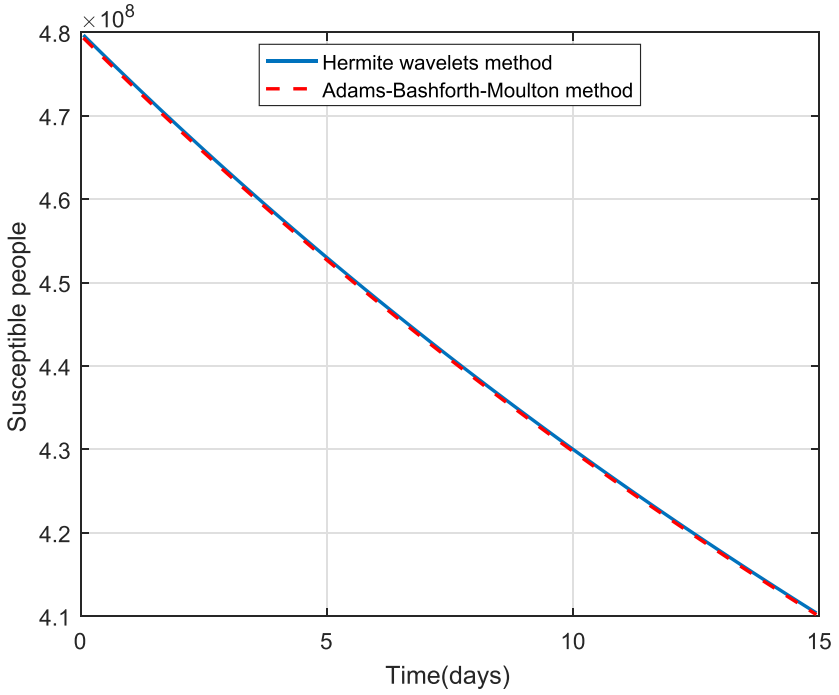

FIGURE 3 Plot of susceptible people for obtained solutions by HWM and ABM at $M = 4$, $k = 6$, and $\alpha = 1$ [Colour figure can be viewed at wileyonlinelibrary.com]

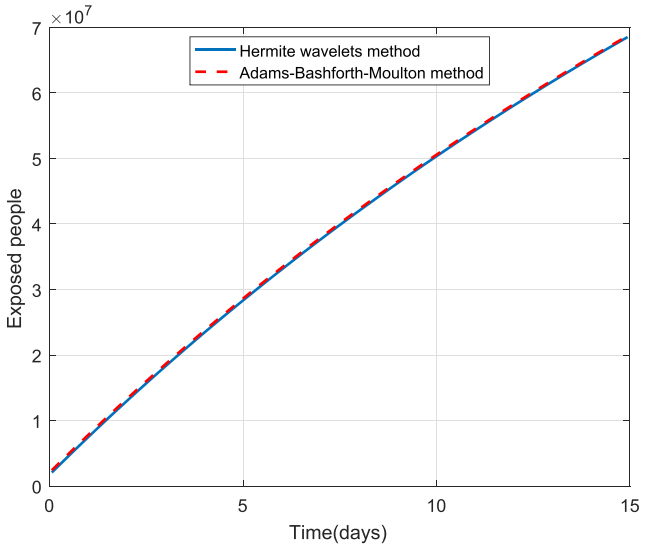

FIGURE 4 Plot of exposed people for obtained solutions by HWM and ABM at $M = 4$, $k = 6$, and $\alpha = 1$ [Colour figure can be viewed at wileyonlinelibrary.com]

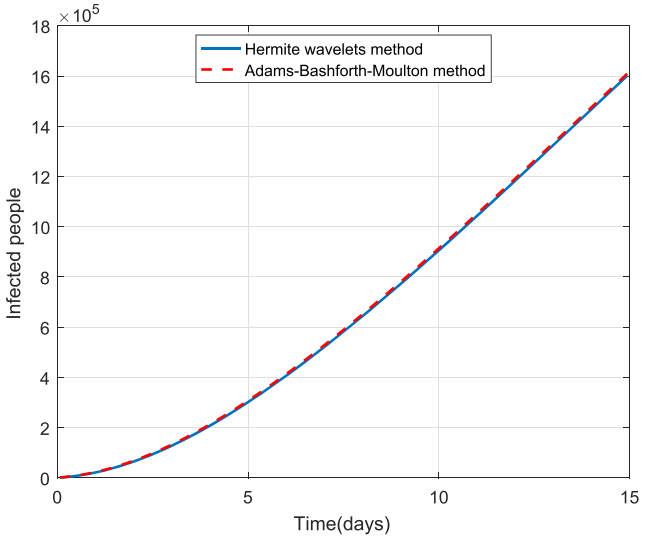

FIGURE 5 Plot of infected people for obtained solutions by HWM and ABM at $M = 4$, $k = 6$, and $\alpha = 1$ [Colour figure can be viewed at wileyonlinelibrary.com]

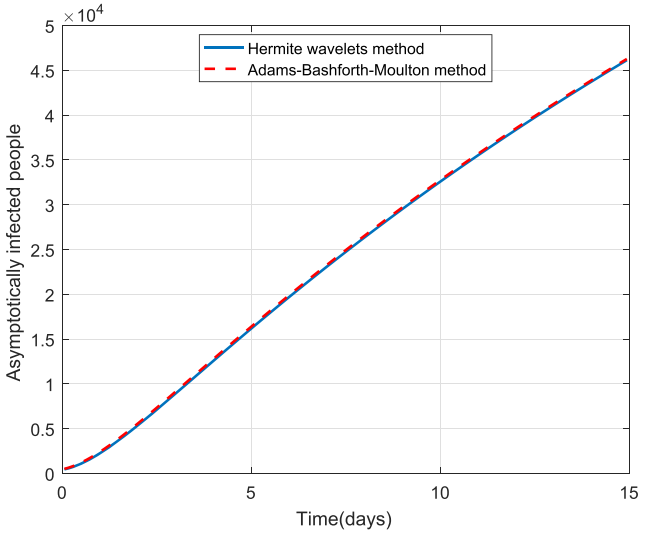

FIGURE 6 Plot of asymptotically infected people for obtained solutions by HWM and ABM at $M = 4$, $k = 6$, and $\alpha = 1$ [Colour figure can be viewed at wileyonlinelibrary.com]

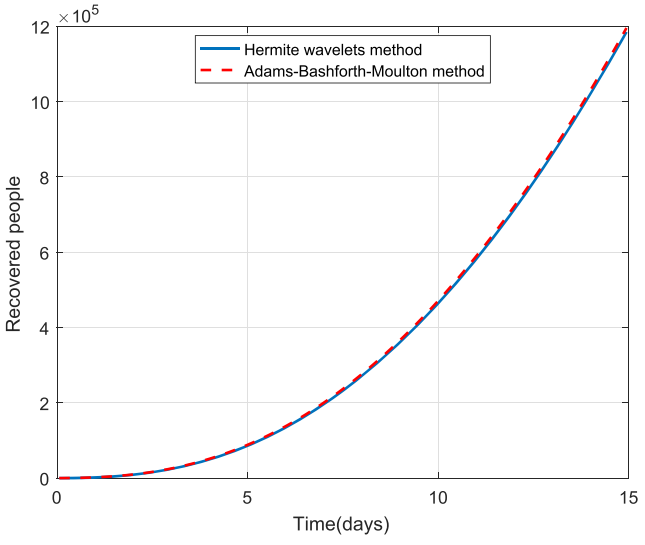

FIGURE 7 Plot of recovered people for obtained solutions by HWM and ABM at $M = 4$, $k = 6$, and $\alpha = 1$ [Colour figure can be viewed at wileyonlinelibrary.com]

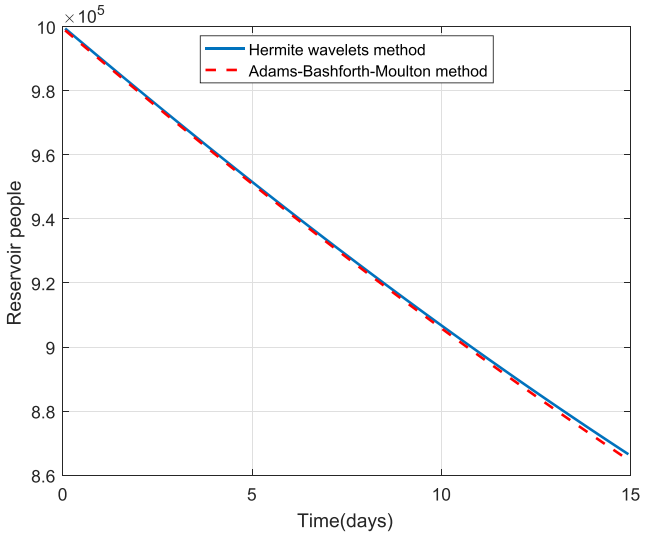

FIGURE 8 Plot of reservoir people for obtained solutions by HWM and ABM at $M = 4$, $k = 6$, and $\alpha = 1$ [Colour figure can be viewed at wileyonlinelibrary.com]

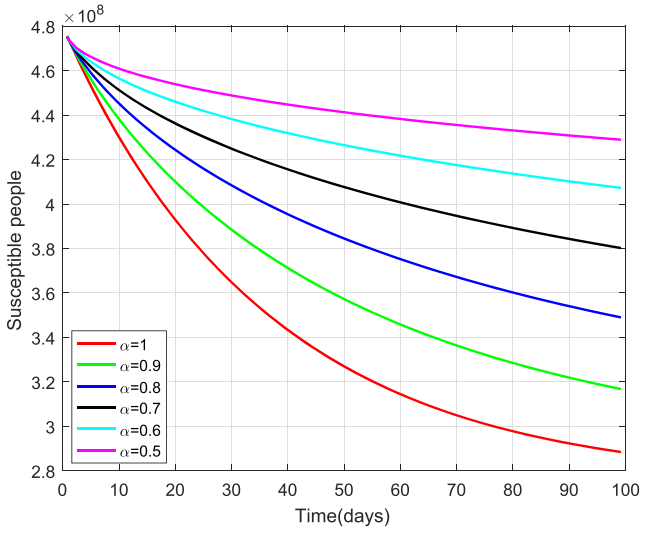

FIGURE 9 Plot of susceptible people for different values of α [Colour figure can be viewed at wileyonlinelibrary.com]

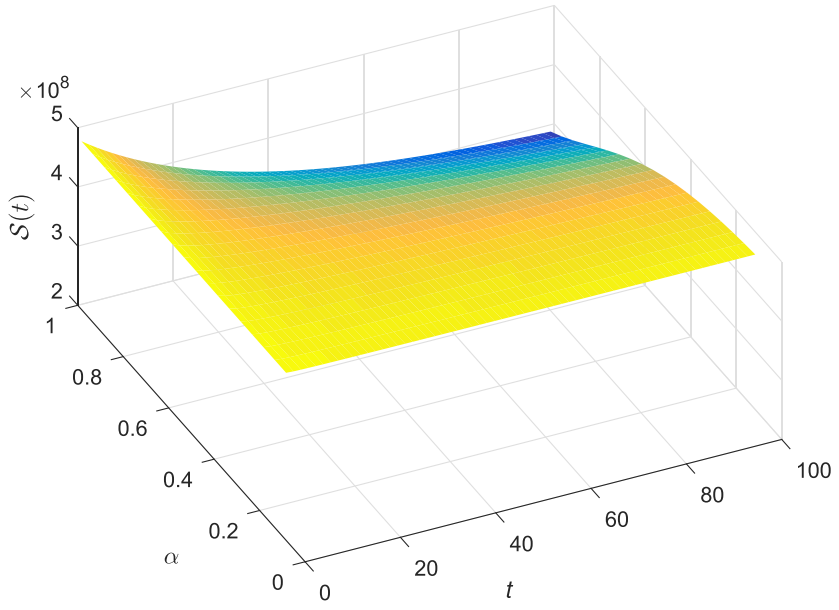

FIGURE 10 Surface plot of susceptible people for $0 < \alpha < 1$ and $0 \le t \le 100$ [Colour figure can be viewed at wileyonlinelibrary.com]

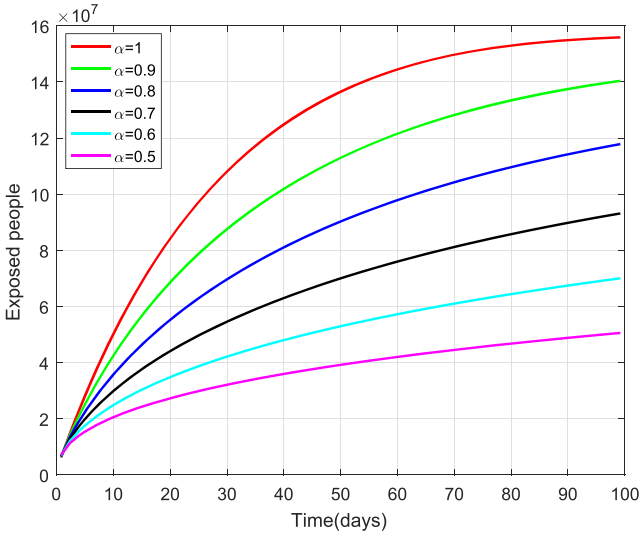

FIGURE 11 Plot of exposed people for different values of α [Colour figure can be viewed at wileyonlinelibrary.com]

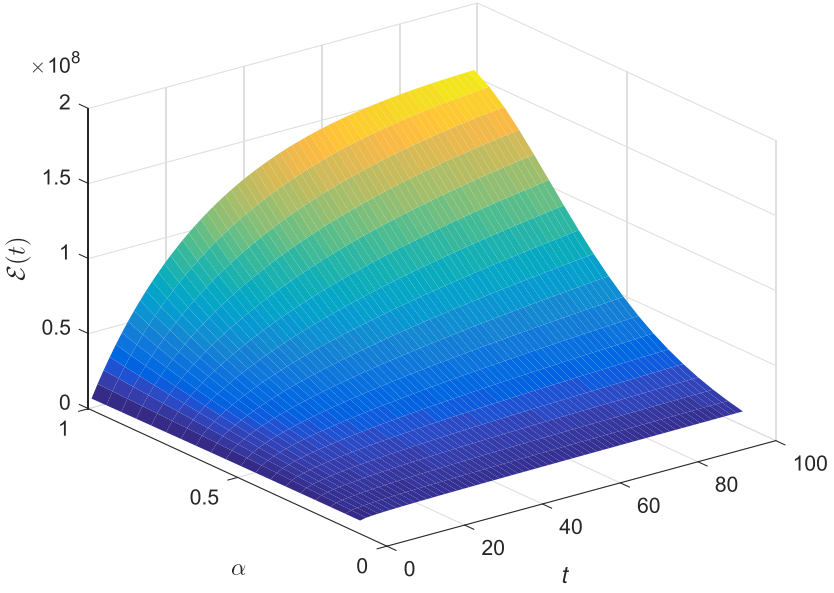

FIGURE 12 Surface plot of exposed people for $0 < \alpha < 1$ and $0 \leq t \leq 100$ [Colour figure can be viewed at wileyonlinelibrary.com]

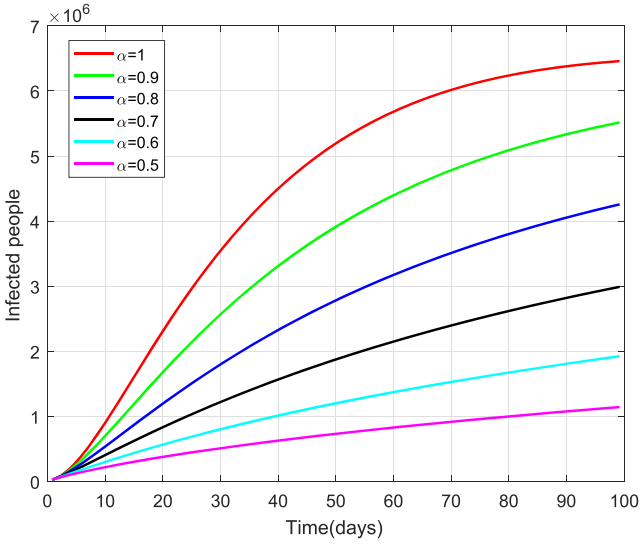

FIGURE 13 Plot of infected people for different values of α [Colour figure can be viewed at wileyonlinelibrary.com]

then total mortality percentage $\lambda = 1/69.50$ per year. The Birth percentage is $\Delta = \mathcal{N} \times \lambda = 6931614.27$ (estimated), contact percentage $(\varphi) = 0.25$, transmission rate $(\beta) = 0.5944$, development duration $(\delta) = 0.0047876$, incubation duration $(\mu) = 0.05$, the ratio of asymptomatic infection $(\phi) = 0.01243$, infection transmission coefficient $(\gamma) = 0.1231 \times 10^7$, readjustment percentage of $\mathcal{I}$ $(\sigma) = 0.09871$, recovery percentage of $\mathcal{A}$ $(\rho) = 0.854302$, share of the infection to $\mathcal{Q}$ by $\mathcal{I}$ $(\xi) = 0.000398$, contribution of the infection to $\mathcal{Q}$ by $\mathcal{A}$ $(\zeta) = 0.001$, and erasing percentage of infection to $\mathcal{Q}$ $(\eta) = 0.01$ in which parameters are either estimated or fitted.[5] The numerical solutions obtained by Hermite wavelets method and ABM are displayed in Figures 3–8. Further, we noticed that the arbitrary-order derivative has a remarkable effect on the dynamics of COVID-19. Susceptible individual $\mathcal{S}(t)$, exposed individual $\mathcal{E}(t)$, infected individual $\mathcal{I}(t)$, asymptotic infected individual $\mathcal{A}(t)$, recovered individual $\mathcal{R}(t)$, and individual in reservoir $\mathcal{Q}(t)$ against time t in days for large amounts of α are displayed in Figures 9–20. Moreover, we observe that the fractional operator provides more flexibility than the integer operator. It is observed that the COVID-19 infection mathematical model depends on time fractional derivative; the current study may guidance to figure out the harmful virus.

Illustration 3 displays behaviors of susceptible peoples by using Hermite wavelet method, and a comparison study through Illustration 1 represented between susceptible peoples in arbitrary-order COVID-19 infection system by using Hermite wavelet and ABM methods at $M = 4, k = 6$, and $\alpha = 1$. The number of susceptible peoples is decreasing in arbitrary-order COVID-19 infection system. We observed that nature of the susceptible peoples is identical by both schemes. Illustrations 4–7 display the nature of exposed, infected, asymptotically infected, and recovered peoples in

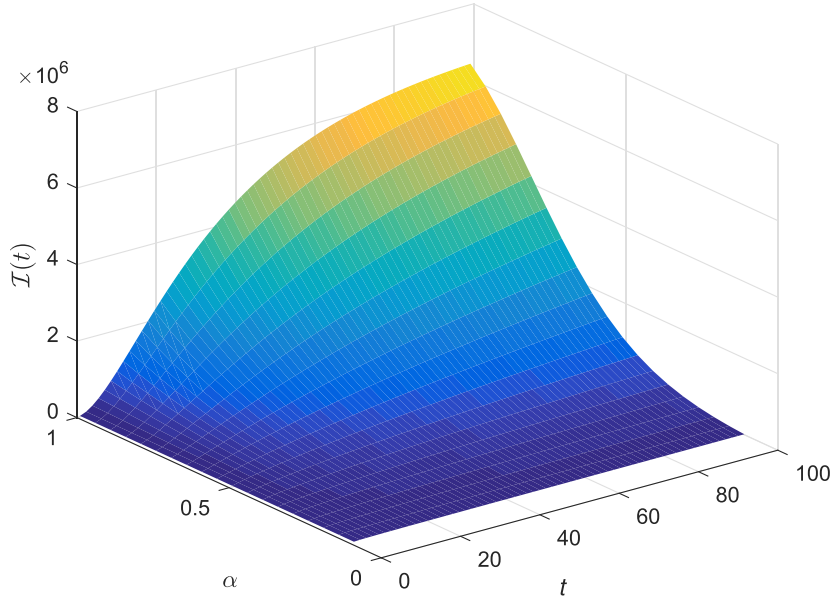

FIGURE 14 Surface plot of asymptotically infected people for $0 < \alpha < 1$ and $0 \le t \le 100$ [Colour figure can be viewed at wileyonlinelibrary.com]

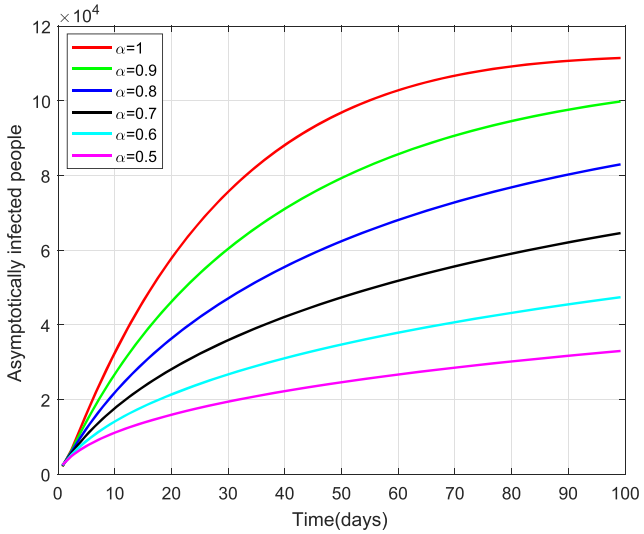

FIGURE 15 Plot of asymptotically infected people for different values of α [Colour figure can be viewed at wileyonlinelibrary.com]

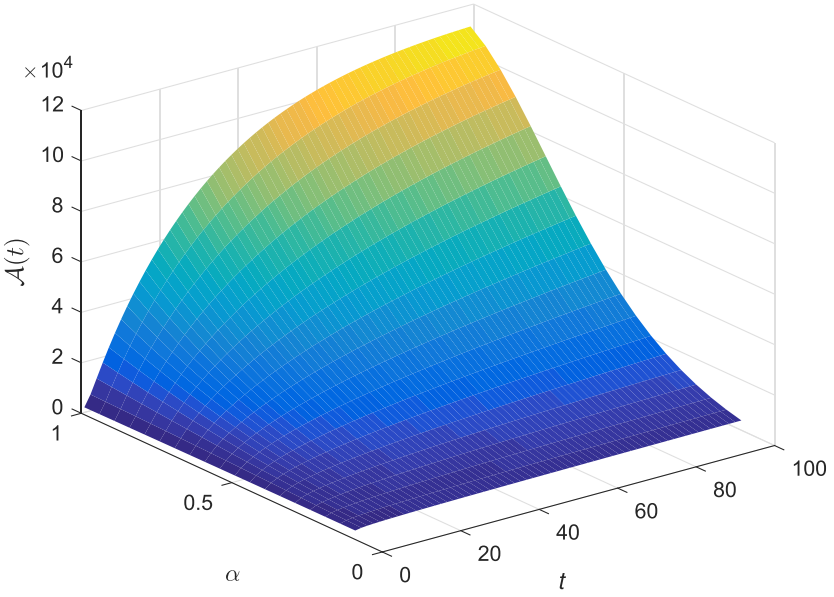

FIGURE 16 Surface plot of asymptotically infected people for $0 < \alpha < 1$ and $0 \leq t \leq 100$ [Colour figure can be viewed at wileyonlinelibrary.com]

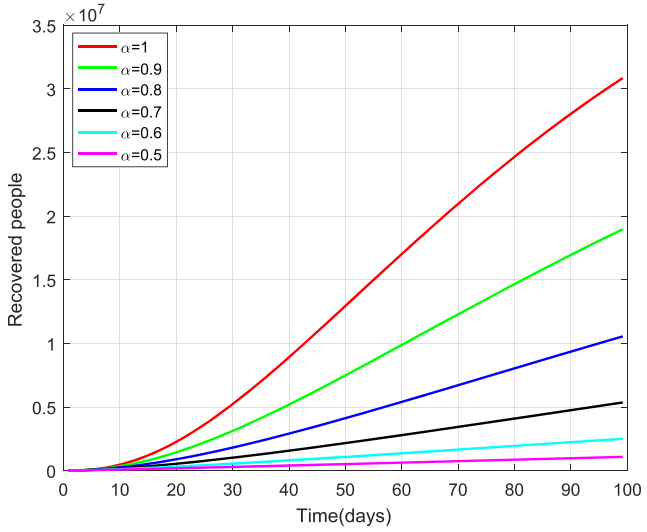

FIGURE 17 Plot of recovered people for different values of α [Colour figure can be viewed at wileyonlinelibrary.com]

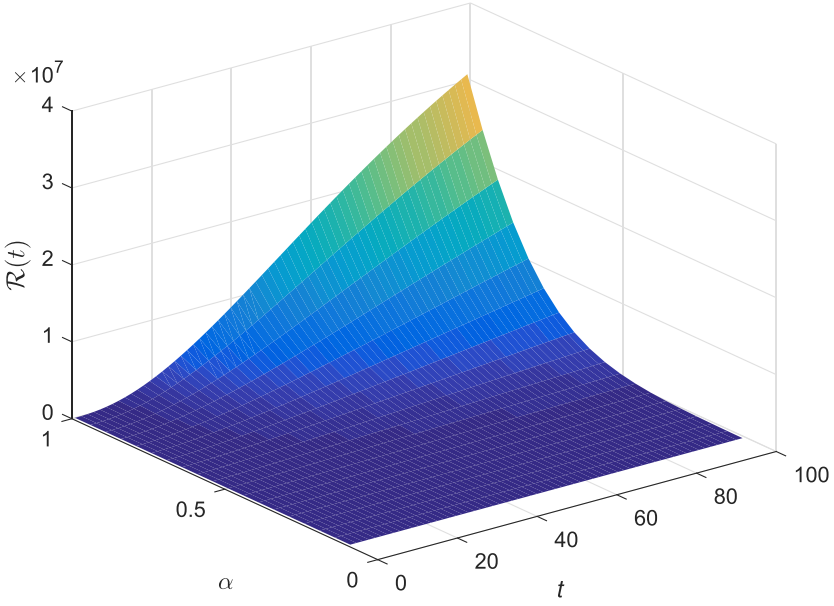

FIGURE 18 Surface plot of recovered people for $0 < \alpha < 1$ and $0 \leq t \leq 100$ [Colour figure can be viewed at wileyonlinelibrary.com]

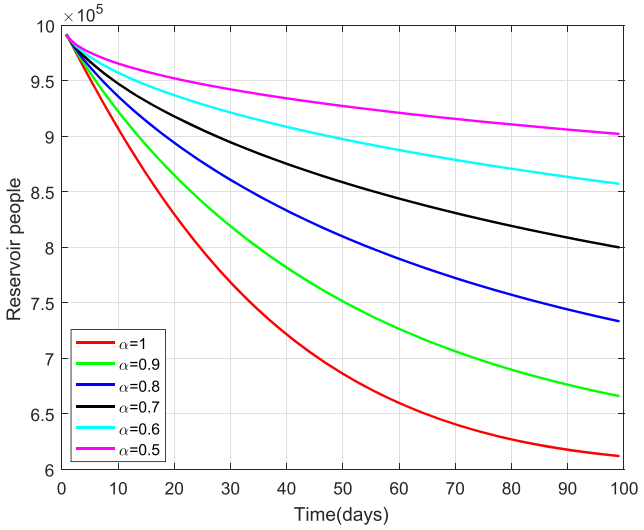

FIGURE 19 Plot of reservoir people for different values of α [Colour figure can be viewed at wileyonlinelibrary.com]

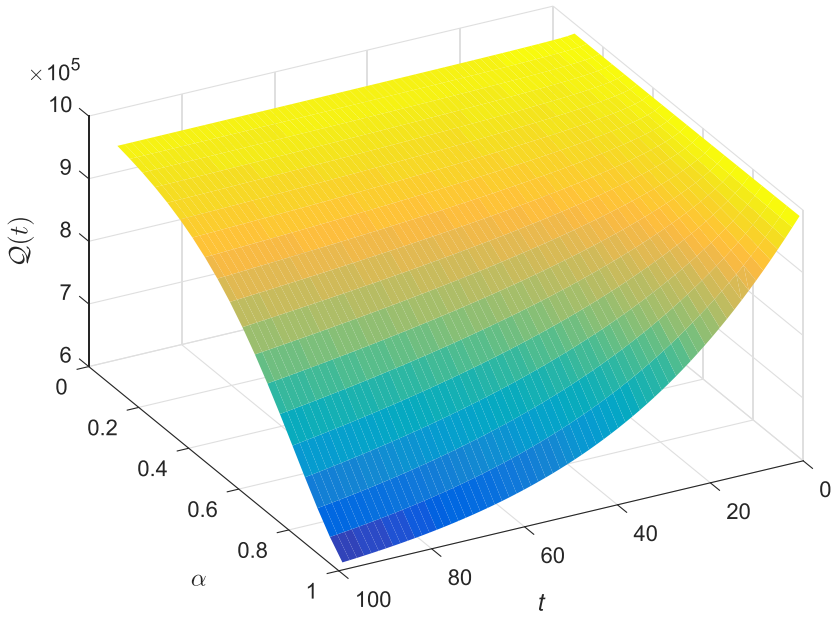

FIGURE 20 Surface plot of reservoir people for $0 < \alpha < 1$ and $0 \leq t \leq 100$ [Colour figure can be viewed at wileyonlinelibrary.com]

arbitrary-order COVID-19 infection system by using Hermite wavelet and ABM methods at $M = 4, k = 6$, and $\alpha = 1$. Further, we observed through Illustrations 4–7 that the number of exposed, infected, asymptotically infected, and recovered peoples is continuously increasing in arbitrary-order COVID-19 infection system, but it is also notice from figure 7 that the total number of recovered peoples is increasing very fast according time. It is also observed through monthly serological survey on COVID-19 that the total number recovery peoples has been jumped. The recovery rate stands at 64.53% among COVID-19 patients. Further, various nature of susceptible, exposed, infected, and recovered individuals in arbitrary-order COVID-19 infection system represented by various Figures 8–20.

7 | CONCLUSION

Novel coronavirus is a extremely infectious infection worldwide. The thousand certified cases and thousands of infection have been reported in various countries. The infection has turn into outbreak, disturbing almost all countries of the world, and has caused enormous budgetary, social, and psychological load on countries. In this article, the COVID-19 infection mathematical model has been determined numerically via Hermite wavelets scheme. Moreover, solutions obtained by Hermite wavelets are compared with solutions obtained by ABM predictor corrector scheme. Firstly, Hermite wavelets function approximation and convergence investigation have been recommended. In other way, an arbitrary-order integral

operator for $[0, t_l]$ has been derived by which the COVID-19 infection can be reconstructed into simply determined system of algebraic equations. Finally, we have analyzed the results through graphically.

It was concluded that susceptible peoples contract the infection through direct contact with infected individuals, as well as indirectly through the presence of coronavirus in the environment. Further, we have examined through study that there is no best option other than social distancing, isolation, and palliative measures in present time.

ACKNOWLEDGEMENT

This research is supported by Ajman University grant 2020-COVID-19-07.

ORCID

Sunil Kumar https://orcid.org/0000-0003-0620-1068

REFERENCES

1. World Health Organization. Coronavirus disease 2019. https://www.who.int/emergencies/diseases/novel-coronavirus-2019; 2020.
2. Editorial. The continuing 2019-ncov epidemic threat of novel coronaviruses to global health—the latest 2019 novel coronavirus outbreak in Wuhan, China. *Int J Infect Dis*. 2020;91(1):264-266.
3. Lin Q, Zhao S, Gao D, et al. A conceptual model for the coronavirus disease 2019 (COVID-19) outbreak in Wuhan, China with individual reaction and governmental action. *Int J Infect Dis*. 2020;93:211-216.
4. Chen T-M, Rui J, Wang Q-P, Zhao Z-Y, Cui J-A, Yin L. A mathematical model for simulating the phase-based transmissibility of a novel coronavirus. *Infect Dis Poverty*. 2020;9(1):1-8.
5. Khan MA, Atangana A. Modeling the dynamics of novel coronavirus (2019-ncov) with fractional derivative. *Alex Eng J*. 2020;59(4):2379-2389.
6. World Health Organization. "Who covid-19 situation report 29". PDF; 2020.
7. Volpert V, Banerjee M, Petrovskii S. On a quarantine model of coronavirus infection and data analysis. *Math Model Nat Pheno*. 2020;15:24.
8. Kucharski AJ, Russell TW, Diamond C, et al. Early dynamics of transmission and control of covid-19: a mathematical modelling study. *Lancet Infect Dis*. 2020;20(5):553-558. https://doi.org/10.1016/S1473-3099(20)30144-4
9. Ahmed I, Baba IA, Yusuf A, Kumam P, Kumam W. Analysis of Caputo fractional-order model for COVID-19 with lockdown. *Adv Differ Equ*. 2020;2020(1):1-14.
10. Gao W, Baskonus HM, Shi L. New investigation of bats-hosts-reservoir-people coronavirus model and application to 2019-ncov system. *Adv Differ Equ*. 2020;2020(1):1-11.
11. Podlubny I. *Fractional Differential Equations: An Introduction to Fractional Derivatives, Fractional Differential Equations, to Methods of their Solution and Some of their Applications*. Academic Press: Elsevier; 1998.
12. Kumar S, Kumar R, Singh J, Nisar KS, Kumar D. An efficient numerical scheme for fractional model of HIV-1 infection of CD4+ T-cells with the effect of antiviral drug therapy. *Alex Eng J*. 2020;59(4):2053-2064.
13. Kumar S, Kumar R, Agarwal RP, Samet B. A study of fractional Lotka-Volterra population model using Haar wavelet and Adams-Bashforth-Moulton methods. *Math Methods Appl Sci*. 2020;43(7):4460-4471.
14. Ghanbari B, Kumar S, Kumar R. A study of behaviour for immune and tumor cells in immunogenetic tumour model with non-singular fractional derivative. *Chaos Soliton Fract*. 2020;133:109619.
15. Mohammadi F, Moradi L, Baleanu D, Jajarmi A. A hybrid functions numerical scheme for fractional optimal control problems: Application to nonanalytic dynamic systems. *J Vib Control*. 2018;24(21):5030-5043.
16. Jajarmi A, Baleanu D. On the fractional optimal control problems with a general derivative operator. *Asian J Control*. 2019:1-10. https://doi.org/10.1002/asjc.2282
17. Sajjadi SS, Baleanu D, Jajarmi A, Pirouz HM. A new adaptive synchronization and hyperchaos control of a biological snap oscillator. *Chaos Soliton Fract*. 2020;138:109919.
18. Jajarmi A, Yusuf A, Baleanu D, Inc M. A new fractional HRSV model and its optimal control: a non-singular operator approach. *Physica A-Stat Mech Appl*. 2020;547:123860.
19. Qureshi S, Yusuf A. Modeling chickenpox disease with fractional derivatives: from caputo to atangana-baleanu. *Chaos Solitons Fractals*. 2019;122:111-118.
20. Baba IA, Olamilekan LI, Yusuf A, Baleanu D. Analysis of meningitis model: a case study of northern Nigeria. *AIMS Bioeng*. 2020;7(4):179.
21. Qureshi S, Yusuf A, Ali Shaikh A, Inc M, Baleanu D. Mathematical modeling for adsorption process of dye removal nonlinear equation using power law and exponentially decaying kernels. *Chaos: An Interdisciplinary J Nonlinear Sci*. 2020;30(4):043106.
22. Srivastava MH, Ahmad H, Ahmad I, Thounthong P, Khan NM. Numerical simulation of three-dimensional fractional-order convection-diffusion pdes by a local meshless method. *Therm Sci*. 2020:210-210.
23. Ahmad I, Ahmad H, Thounthong P, Chu Y-M, Cesarano C. Solution of multi-term time-fractional pde models arising in mathematical biology and physics by local meshless method. *Symmetry*. 2020;12(7):1195.

24. Inc M, Khan MN, Ahmad I, Yao S-W, Ahmad H, Thounthong P. Analysing time-fractional exotic options via efficient local meshless method. *Results Phys*. 2020;19:103385.
25. Ravichandran C, Logeswari K, Panda SK, Nisar KS. On new approach of fractional derivative by Mittag–Leffler kernel to neutral integro-differential systems with impulsive conditions. *Chaos Soliton Fract*. 2020;139:110012.
26. Valliammal N, Ravichandran C, Nisar KS. Solutions to fractional neutral delay differential nonlocal systems. *Chaos Soliton Fract*. 2020;138:109912.
27. Panda SK, Abdeljawad T, Ravichandran C. A complex valued approach to the solutions of Riemann–Liouville integral, atangana-baleanu integral operator and non-linear telegraph equation via fixed point method. *Chaos Soliton Fract*. 2020;130:109439.
28. Solís-Pérez JE, Gómez-Aguilar JF, Atangana A. A fractional mathematical model of breast cancer competition model. *Chaos Soliton Fract*. 2019;127:38-54.
29. Ullah S, Khan MA, Farooq M. A new fractional model for the dynamics of the Hepatitis B virus using the Caputo-Fabrizio derivative. *Eur Phys J Plus*. 2018;133(6):237.
30. Agarwal P, Singh R. Modelling of transmission dynamics of nipah virus (niv): a fractional order approach. *Physica A: Stat Mech Appl*. 2020;547:124243.
31. Kilicman A, Hamdan NI. A fractional order SIR epidemic model for dengue transmission. *Chaos Soliton Fract*. 2018;114:55-62.
32. Dubey VP, Kumar R, Kumar D. Numerical solution of time fractional three-species food Chain model arising in the realm of mathematical ecology. *Int J Biomath*. 2020;13(2):2050011.
33. Baba IA, Ghanbari B. Existence and uniqueness of solution of a fractional order tuberculosis model. *Eur Phys J Plus*. 2019;134(10):489.
34. Gao Z, Wood JG, Burgess MA, Menzies RI, McIntyre PB, McIntyre CR. Models of strategies for control of rubella and congenital Rubella syndrome a 40 year experience from Australia. *Vaccine*. 2013;31(4):691-697.
35. Beylkin G, Coifman R, Rokhlin V. Fast wavelet transforms and numerical algorithms 1. *Commun Pure Appl Math*. 1991;44(2):141-183.
36. Lakestani M, Razzaghi M, Dehghan M. Semiorthogonal spline wavelets approximation for Fredholm integro-differential equations. *Math Probl Eng*. 2006;2006:096184. https://doi.org/10.1155/MPE/2006/96184
37. Chui CK. *Wavelets: A Mathematical Tool for Signal Analysis*, Vol. 1: SIAM; 1997.
38. Shiralashetti SC, Kumbinarasaiah S. Theoretical study on continuous polynomial wavelet bases through wavelet series collocation method for nonlinear Lane–Emden type equations. *Appl Math Comput*. 2017;315:591-602.
39. Umer S. Hermite wavelet method for fractional delay differential equations. *J Difference Equ*. 2014:359093. https://doi.org/10.1155/2014/359093
40. ur Rehman M, Khan RA. The Legendre wavelet method for solving fractional differential equations. *Commun Non Sci Num Simulation*. 2011;16(11):4163-4173.
41. Yuttanan B, Razzaghi M. Legendre wavelets approach for numerical solutions of distributed order fractional differential equations. *Appl Math Model*. 2019;70:350-364.
42. Wang J, Xu T-Z, Wei Y-Q, Xie J-Q. Numerical simulation for coupled systems of nonlinear fractional order integro-differential equations via wavelets method. *Appl Math Comput*. 2018;324:36-50.
43. Kumar S, Ahmadian A, Kumar R, et al. An efficient numerical method for fractional SIR epidemic model of infectious disease by using Bernstein wavelets. *Mathematics*. 2020;8(4):558.
44. Mundewadi RA, Kumbinarasaiah S. Numerical solution of Abel's integral equations using Hermite wavelet. *Applied Math Non Sci*. 2019;4(1):181-192.
45. Shiralashetti SC, Kumbinarasaiah S. Hermite wavelets operational matrix of integration for the numerical solution of nonlinear singular initial value problems. *Alex Eng J*. 2018;57(4):2591-2600.
46. Farman M, Akgül A, Ahmad A, Imtiaz S. Analysis and dynamical behavior of fractional-order cancer model with vaccine strategy. *Math Methods Appl Sci*. 2020;43(7):4871-4882.
47. Akgül A, Modanli M. Crank–Nicholson difference method and reproducing kernel function for third order fractional differential equations in the sense of Atangana–Baleanu Caputo derivative. *Chaos Soliton Fract*. 2019;127:10-16.
48. Bhatter S, Mathur A, Kumar D, Singh J. A new analysis of fractional Drinfeld–Sokolov–Wilson model with exponential memory. *Physica A: Stat Mech Appl*. 2020;537:122578.
49. Mehrdoust F, Sheikhani AHR, Mashoof M, Hasanzadeh S. Block-pulse operational matrix method for solving fractional Black-Scholes equation. *J Econ Stud*. 2017;44(3):489-502.
50. Ebadian A, Khajehnasiri AA. Block-pulse functions and their applications to solving systems of higher-order nonlinear Volterra integro-differential equations. *Electron J Differ Equ*. 2014;54:1-9.
51. Li Y, Sun N. Numerical solution of fractional differential equations using the generalized block pulse operational matrix. *Com Math Appl*. 2011;62(3):1046-1054.
52. Srivastava M, Agrawal SK, Das S. Synchronization of chaotic fractional order Lotka–Volterra system. *Int J Nonlinear Sci*. 2012;13(4):482-494.
53. Diethelm K, Ford NJ, Freed AD. Detailed error analysis for a fractional Adams method. *Numer Algorithms*. 2004;36 (1):31-52.

How to cite this article: Kumar S, Kumar R, Momani S, Hadid S. A study on fractional COVID-19 disease model by using Hermite wavelets. *Math Meth Appl Sci*. 2021;1–17. https://doi.org/10.1002/mma.7065